Experimental Investigation of Transparent Parabolic Trough Collector Based on Gas-Phase Nanofluid

Marco Potenza, Marco Milanese[a], Gianpiero Colangelo, Arturo de Risi

[1]Department of Engineering for Innovation, University of Salento, SP per Monteroni, Lecce (Italy)

[a]marco.milanese@unisalento.it, +39 0832297760

Abstract

An experimental study on new high temperature parabolic trough collector (PTC), with transparent receiver tube, based on gas-phase nanofluid, has been carried out for the first time in this work. Two-axes solar tracking PTC, with 4 m^2 reflecting surface has been realized. Besides, two coaxial quartz tubes, with vacuum in the inner space were used as receiver pipe, with air-dispersed CuO nano-powders as working fluid. The aim of this work was to investigate the technological issues related to the use of gas-based nanofluid coupled with transparent quartz receiver and to evaluate the performance of the first prototype, comparing numerical and experimental results. The experimental campaign highlighted a critical issue related to nanopowder deposition within the receiver pipe, due to humidity. Moreover, in a day of measurement, the fluid temperature higher than 145°C has been maintained for about 10 hours, reaching a maximum value of 180 °C, with a mean efficiency of about 65%.

Keywords: Parabolic Trough Collector, Nanoparticles, Gas-phase Nanofluids, Transparent Receiver Tube

Nomenclature

a	aperture of mirror [m];
C_p	specific heat capacity [J/kg K]
d	diameter of receiver tube [m];
f	focal length of mirror [m];
I_b	solar radiation [W/m^2];
I_t	solar radiation passing through the receiver [W/m^2];
k	wave number;
$K_{\alpha\gamma}$	angular factor;
$\dot{H}_{abs}$	heat rate incident absorbed by heat transfer fluid [W];
$\dot{H}_{inc}$	heat rate incident on the receiver [W];

$\dot{H}_{loss}$ heat rate loss with the surroundings [W];

$\dot{H}_{inc}$ heat rate incident on receiver [W];

L length of receiver tube [m];

$\dot{m}_{NF}$ mass flow rate of *NF* [kg/s];

m nanoparticles complex refractive index;

N number of nanoparticles per unit volume;

r mean radius of nanoparticles;

R thermal resistivity of receiver tube [K/W m];

S area of the mirror [m^2];

S_I effective area of the mirror [m^2];

t global receiver transmittance;

T_{env} environmental temperature [K];

T_{in} inlet temperature [K];

T_{NF} temperature of *NF* [K];

T_{out} outlet temperature [K];

W minimum diameter of the receiver tube [m];

Greek letters

α global receiver absorptance;

γ shape factor;

ε mean optical efficiency;

η solar to thermal efficiency;

θ incident radiation angle [°];

θ_r rim angle [°];

ρ_s mirror reflectivity;

τ *NF* trasmissivity;

1. Introduction

In recent years, several types of parabolic trough collector (PTC) have been largely investigated and tested, renewing worldwide interest in this technology, that is suitable for electric power generation [1]-[4].

As known, PTC is the most common type of concentrating solar power technology. These systems typically use synthetic oil or molten salts as heat transfer fluid. Notwithstanding its characteristics

of flammability and toxicity and its relatively low maximum working temperature (<400 °C), synthetic oil represents the most common heat transfer fluid in PTC power plants [5].

On the other hand, molten salts, while can work up to 600 °C [5]-[8], require expensive anti-freezing systems because of their solidification temperature of about 220 °C [9],[10].

To overwhelm the limitations of synthetic oil and molten salts, according to de Risi *et al.* [11], in this work the authors proposed to use gas-phase nanofluid as heat transfer fluid in parabolic trough collector, with transparent receiver tube (named transparent parabolic trough collector, TPTC). The main difference between traditional opaque and innovative transparent receiver is related to the heat transfer mechanism between solar radiation and working fluid: in the first case the fluid is heated by thermal convection through the opaque receiver tube, while in the second case, the nanofluid is directly irradiated and heated by solar radiation. Several studies conducted on direct absorption liquid based nanofluids demonstrated advantages of direct absorption with respect to indirect one [12]-[15].

In recent years, numerous works have been carried out on thermal conductivity and heat transfer in nanofluids [16]-[26]. Furthermore, the high absorption coefficient of solar radiation, which characterizes different nanofluids [27]-[32] has been the inspiration for several studies. About that, Miller and Koenigsdorff [33] presented a thermal model of solar central receiver that volumetrically absorbs concentrated sunlight directly in flowing gas stream seeded with submicron carbon particles, while Bertocchi *et al.* [34] proposed a solar particle receiver, in which the particle/gas energy transfer is concluded within a short path length, which allows compact design and minimal conduction heat losses.

The above-mentioned studies encourage the use of gas-based nanofluid to directly absorb solar radiation, therefore in this paper, for the first time, a lab-scale prototype of TPTC operating with gas-based nanofluid as heat transfer fluid is experimentally investigated. The basic idea was to disperse nanoparticles, characterized by high optical absorbance and heat capacity, within an air steam flow running in a transparent receiver, in order to obtain direct absorption of solar radiation and a subsequent temperature increasing of the nanofluid. Therefore, aim of this work was to evaluate the performance of the prototype and to investigate technological problems related to use of gas-based nanofluid coupled with transparent quartz receiver. Finally, by comparing numerical and experimental results, the mathematical model of TPTC, developed in [11], has been validated.

2. Description of the system

A lab-scale prototype of TPTC has been realized in Lecce (Italy), according to the results of a previous numerical study on direct absorption solar power systems [11]. The prototype consists essentially of 4 m^2 TPTC, with blower for air-based nanofluid movement, heat dissipator,

nanoparticles injection system and pressure regulation system to ensure constant pressure into the nanofluid circuit. In Figure 1 and Figure 2 a schematic layout and a picture of the prototype are shown, respectively.

In the main circuit (red line in Figure 2), the air-based nanofluid is forced to pass through the transparent receiver by means of a blower. To compensate the increment of volume, related to the increase in temperature, ensuring constant pressure into the circuit, two water tanks, $Tank_1$ and $Tank_2$ connected with a bidirectional pump have been used (pressure regulation system in Figure 2). The control system modifies the water level within the $Tank_1$ and subsequently the air volume, according to the measured pressure. A particles separator ensures no contamination between nanofluid circuit and water tank. The particles are loaded into the prototype by means of an injection system positioned on the blower intake.

2.1. The transparent receiver

The transparent receiver tube has been developed and realized through two coaxial quartz pipes, with vacuum of about 1 mbar absolute pressure within the annular space. Vacuum has been employed in order to reduce convective heat transfer from the receiver tube to the environment. The inner and outer quartz pipes have been connected together by means of a quartz annulus welded to both, so as to obtain a closed volume (Figure 3a). Therefore, vacuum between the two pipes has been done by means of a mechanical pump connected to the quartz probe, shown in Figure 3b. Finally, after the vacuum condition has been reached, the quartz probe has been locally heated up to its melting temperature and closed by clamping. In this first prototype, no coating (to reduce radiation heat losses) has been deposited on the quartz tube surface. Table 1 summarizes the main characteristics of the transparent receiver, while in Figure 4 an optical scheme is reported.

In order to characterize the energy loss due to receiver positioning errors and to evaluate the relationship between imperfections of construction and optical performance of the system, a raytracing analysis has been carried out, by means of Opticad software, taking into account, as Sun-like light, a source with a dispersion angle of 0.534°. Figure 5 shows the ray-tracing results for different positionings of the receiver with respect to the base of the mirror.

From the analysis of Figure 5, it can be noticed that a deviation of 10 mm in the collector positioning, with respect to the geometric focus, leads to marked differences in the optical results. This value of deviation represents the precision level needed in construction of TPTC.

2.2. The parabolic mirror

The parabolic mirror is composed by two reflective panels of dimensions 1600x1250 mm, properly curved, to obtain a parabolic profile, whose focus is placed at distance of 1000 mm from the base of

the mirror. Thereby, a linear extension of the parabolic mirror equal to 2500 mm has been obtained. The prototype of TPTC has been designed to withstand a headwind of 140 km/h and a temperature of 550 °C on the receiver and 100 °C on the mirror. Particularly, several FEM calculations have been carried out, according to the reference normative *NTC 2008 – 3.3*, which imposes a wind withstand of 140 km/h coupled with a safety factor of 1.4, for outdoor installations located in Lecce (Italy). Figure 6 a) and b) show some FEM analysis results in terms of maximum deformation and Von Mises stress under the effects of high speed wind conditions (140 km/h). As it can be noticed, the maximum stress is about 80 MPa, below tensile strength of 430 MPa.

The system under investigation is equipped with a tip–tilt dual axis solar tracker, as shown in Figure 6 c), d) and e).

The East–West movement is driven by the turntable Transtecno model ST7, coupled to the engine Transtecno EC070.120, through a worm reducer Transtecno ECP050/523 1/168.84, having a transmission ratio of 7, a maximum output torque of 26 Nm and a maximum rotational speed equal to 18 rpm. The supply voltage is 12 V for a maximum power consumption of 70 W. The vertical movement has been obtained by means of two-combined worm gears with transmission ratio 1/3000, capable of delivering a maximum torque of 65 Nm. The supply voltage is 12 V for a maximum power consumption of 100 W. This system allows rotation of the parabola from a minimum angle of 15° to a maximum of 115°, with respect to the vertical axis for a total angle equal to 100°, as shown in Figure 6 d) and e).

The maximum elevation, 15° less than the Zenith position, is compatible with the maximum sun elevation of 72.5°, at the installation site (latitude 40.336083, longitude 18.1199312). The idle position is used during night hours, in order to reduce formation of dew on the mirror, which could lead to its gradual opacification, resulting in decreased efficiency of the concentrator.

Finally, the prototype is equipped with a unit control system, based on a NI cRIO 9114, provided with 8 IO modules for sensors acquisition, tracking system control and devices actuation. All inputs are directly connected with a 40 MHz FPGA (Field Gate Programmable Array) chip. This system allows:

- to track the Sun and correct the mirror position in real-time, according to the real condition of irradiance;
- to measure pressure and temperature (3 points), according to the scheme in Figure 1;
- to switch on/off the blower, the dissipator and the bidirectional pump (Figure 1).

2.4. The nanofluid

Since solar radiation is directly absorbed by nanofluid (*NF*) in TPTC, optical behavior of nanoparticles (*NPs*) has to be as similar as possible to a black body. In a previous work [16],

authors investigated the optical absorption of several nanofluids at fixed concentration of 0.05%vol. The transmittance comparison reported in Figure 7 shows that the best nanofluid in terms of absorption of solar radiation is based on CuO *NPs*, within the UV-VIS wavelength range.

Therefore, the CuO nanopowders have been directly injected into the solar receiver tube by means of a Venturi pipe (nanoparticles injection system in Figure 1), dispersing them within the air flow, driven by the blower. The selected powder had a Sauter mean diameter of 7.4 nm, as reveled by the Scherrer-XRD analysis in Figure 8.

Finally, from a further SEM analysis, high clustered structures with main dimension up to 10 μm have been found.

3. Mathematical model

In this work, the mathematical model of TPTC developed in [11] has been validated. For the reader convenience, the essential formulation of this model has been reported next, according to the following assumptions:

a) one-dimensional flow within the receiver;
b) negligible conduction losses at the ends of trough (all pipes, valves and other elements constituting the prototype have been insulated);
c) negligible thermal inertia effects (the lab-scale system has a slight mass with respect to the solar power concentrated by the parabolic trough);
d) no positioning errors due to solar TPTC tracking system.

3.1. Optical properties of nanofluids

When light passes through a medium, it is attenuated due to absorption and scattering processes. Taking into account the Beer-Lambert law, it is possible to calculate the global receiver absorptance, α, by means of the following equation [11]:

$$\alpha = 1 - t = 1 - \int_{\lambda} \tau(\lambda)\, d\lambda = 1 - \int_{\lambda} e^{-NdC_{ext}(\lambda)}\, d\lambda \tag{1}$$

Where:

$$C_{ext}(\lambda) = \frac{8}{3} k(\lambda)^4 r^4 \left|\frac{m(\lambda)^2 - 1}{m(\lambda)^2 + 2}\right|^2 \pi r^2 - 4k(\lambda) r \mathrm{Im}\left\{\frac{m(\lambda)^2 - 1}{m(\lambda)^2 + 2}\right\} \pi r^2 \tag{2}$$

With the integral of Eq. (1) that has to be extended to the entire solar spectrum.

Taking into account Eq. (1) and according to the complex refractive index of CuO, $m(\lambda)$, the *NF* trasmissivity, τ, has been calculated, as shown in Figure 9.

As it is possible to observe, the *NF* under investigation absorbs all radiation ($\tau \cong 0$) in the visible region, up to 780 nm, while the trasmissivity increases with the infrared radiation. Taking into account the solar spectrum is composed mainly of visible light, this result encourages the use of CuO-based *NF* as absorbing fluid. As direct consequence of the results of Figure 9, according to the ASTM G173-03 Solar Reference Spectra and taking into account Eq. (1) and (2), Figure 10 shows the calculated receiver quartz tube absorptance as a function of the volumetric concentration of *NPs* within *NF*.

The global receiver absorptance results higher than 70% even at very small volumetric concentration of *NPs*.

3.2. Solar thermal analysis

Due to optical losses and shading effects, solar power, which can be absorbed by heat transfer fluid is a fraction of that incident on the collector and it has been evaluated according to the following mathematical model. As first step, the incident heat rate on the receiver, $\dot{H}_{inc}$, has been calculated as [35]:

$$\dot{H}_{inc} = I_b \, S_I \cos\theta \, \varepsilon \, \alpha \tag{3}$$

Where S_I and ε are defined as [35]:

$$S_I = \left(1 - \frac{d}{a}\right) S \tag{4}$$

$$\varepsilon = \rho_s \, \gamma \, K_{\alpha\gamma} \tag{5}$$

Eq. (4) takes into account that the collector surface actually exposed to solar radiation differs from the real surface because of shading phenomena caused by the receiver, while Eq. (5) explicates the mean optical efficiency of the solar receiver as a function of mirror reflectivity, ρ_s, shape factor, γ and angular factor, $K_{\alpha\gamma}$.

The temperature of the heat transfer fluid at the outlet of the receiver tube has been evaluated by means of the energy conservation equation written as follows [36]:

$$\int_L \dot{H}_{abs}(x)\, dx = \int_L \dot{H}_{inc}(x)\, dx - \int_L \dot{H}_{loss}\,(x)\, dx \tag{6}$$

Where:

$$\int_L \dot{H}_{abs}\,(x)\, dx = \dot{m}_{NF}\, C_p (T_{out} - T_{in}) \tag{7}$$

Therefore, the rate of energy loss with the surroundings ($\dot{H}_{loss}$) has been calculated according to the following equation:

$$\dot{H}_{loss} = \int_L \frac{T_{NF} - T_{env}}{R} dx \tag{8}$$

Where, the thermal resistivity per unit of length of receiver, *R*, has been taken into account according to the equivalent thermal circuit of Figure 11.

The parallels of R1-R2 and R6-R7 represent the convective and radiative resistances on the inner and outer quartz tubes of the receiver. R3 and R5 represent the conductive resistances of the inner and outer quartz tubes, respectively, whereas R4 is the thermal resistance of the vacuum layer.

Finally, the solar to thermal efficiency, η, has been obtained as:

$$\eta = \frac{\dot{H}_{abs}}{\dot{H}_{inc}} \tag{9}$$

Table 2 summarizes the parameters taken into account to perform the numerical analysis of the system under investigation.

The values of *NF* velocity, *NF* mass flow rate and *NPs* volume concentration have been chosen so as to minimize powder deposition within quartz receiver: the higher the velocity, the higher the powder transportation by air flow and the lower the deposition within the pipe. Moreover, velocities higher than 11.5 m/s produce too short particles crossing time of the receiver, leading to a reduction of *NF* temperature at the outlet. Higher values of powder concentration than 0.06 %vol cause high powder deposition on the quartz pipe thus reducing the pipe surface available for nanofluid direct irradiation.

4. Discussion of results

The first objective of the present work was to investigate the technological issues related to the use of gas-based nanofluid coupled with transparent quartz receiver.

The experimental campaign showed nanopowder accumulation within the pipes of the prototype. Particularly, due to high roughness (200-300 μm) of the steel pipes, a high deposition phenomenon has been observed on their inner surface (Figure 12). While, with regards to the quartz tubes, a similar phenomenon, but less intense, has been observed only in the first 50 cm from the inlet section, as shown in Figure 13.

In this case, due to the reduced roughness of quartz, the deposition has been lower than in the metal pipes. Besides, experimental observations showed nanopowder depositions strictly related to flow direction: at the inlet section a swirling component of the flow leads to a particles flow strip, which yields the subsequent quartz tube impingement with nanopowder. Conversely, after about 50 cm from the inlet, the flow becomes fully homogenized, reducing the dirtying of the transparent quartz

pipe. This result is very important, because the dirtying phenomenon can strongly influence TPTC performance, since it reduces the amount of solar radiation directly absorbed by nanofluid.

In Figure 13 c) and d) the nanopowders deposition is shown, close to the inlet section, before the first run and after 900 hours of operation.

Another problem, which is occurred during experimental campaign, was related to high hydrophilicity of CuO nanopowders [37],[38]. Particularly, due to air humidity in the air-based nanofluid, the CuO powders bound with water, forming $Cu(OH)_2$ that increases the deposition phenomenon on the inner pipes surface, proportionally to the presence of hydroxyl ion [39],[40].

To deeply investigate the content of water bounded to CuO nanoparticles, a FTIR analysis has been done, comparing the raw material with the nanopowder subjected to about 300 hours of tests (Figure 14).

The FTIR spectrum reveals two different transmission valleys, at 1419 cm^{-1} and 948 cm^{-1}, more evident on the CuO-*NPs* spectrum, that correspond to the bending bonds of the OH hydroxyl ion of water [41],[42].

The presence of water into the closed-loop *NF* circuit was due to the water-based pressure compensation system ($Tank_1$ and $Tank_2$ in Figure 2a) that is connected to the main circuit by means of a *NPs* separator.

According to these experimental evidences, the first conclusion of this work was that all components of TPTC based on gas-phase *NF* have to be water-free in order to minimize deposition phenomenon.

The second objective of the present work was to evaluate the performance of the prototype under investigation. In the following, the results of an experimental test, carried out in a mid-May day are shown. This period of the year has been chosen as reference, because the solar radiation is not at the maximum reachable during summer solstice and the weather conditions are good and frequently sunny.

Figure 15 shows the *NF* temperature, measured at 3 different points of the prototype, according to Figure 2a. Furthermore, the solar radiation, registered during the test, has been reported.

As shown in Figure 15, at the outlet of the transparent receiver (T_3), the maximum reached temperature was 183°C, while the temperature higher than 145°C has been maintained for about 10 hours, with 12 hours of useful solar radiation during the test day. This temperature value is enough to integrate the TPTC system with a low size ORC power generator. For low scale ORC with scroll expander and working with R245fa fluid, in fact, the temperature of 145°C allows maximization of power plant productivity [43]. Moreover, in cogeneration ORC systems, heat sources can be used

down to a temperature of about 80°C [44]-[46], so that the proposed TPTC can be highly recommended.

In Figure 16 the influence of cloudy weather on *NF* temperature is shown. The solar radiation decreased for about 15 minutes due to a cloud shadowing the collector: in this period of time the temperature T_3, at the outlet of the transparent receiver, went down sharply with a reduction of about 40°C. The temperature T_2, at the blower inlet, was less affected by clouds and a reduction of about 20°C was registered. Finally, at the transparent receiver inlet (T_1), no influence of solar radiation reduction was detected.

This result demonstrates that thermal inertia is very different between TPTC and opaque PTC: the traditional receiver has higher thermal inertia because solar radiation is absorbed by the steel pipe and then transferred to the fluid [47],[48]. Instead, as discussed before, in TPTC, solar radiation directly heats the air-based nanofluid and so clouds can lead to quasi-zero the thermal source (the sun), pushing down the *NF* temperature.

In the last part of this work, by comparing numerical and experimental results, the mathematical model of TPTC has been validated. Figure 17 shows the comparison between experimental and calculated outlet temperature T3 in the prototype, while Figure 18 is referred to the efficiency of the prototype.

The numerical model allows predicting with good approximation the working parameters of the system under investigation. The differences between experimental and measured curves in Figure 17 and Figure 18 can be explained taking into account the assumptions on which the mathematical model is based.

In the last step of this work, the optical efficiency decay of the receiver as a function of time, due to *NPs* deposition, has been evaluated. As can be expected, quartz receiver pipe transparency plays a fundamental role in *NF* heating and solar radiation conversion efficiency. Actually, the optical efficiency of the receiver in transmitting light to the nanofluid is related to powders deposition on the internal side of the transparent pipe: the higher the deposition the lower the efficiency. The powder on the transparent tube reduces the amount of solar radiation directly absorbed by nanofluid and subsequently its temperature. In Figure 19, the optical efficiency of the transparent receiver at the inlet and outlet section is reported, as a function of time of operation.

According to the experimental results of Figure 13, Figure 19 confirms higher powder deposition at the receiver inlet with respect to the outlet. Therefore, these results suggest that a cleaning operation has to be periodically done in order to ensure high solar to thermal conversion efficiency for long periods of time.

5. Conclusions

In this work, an innovative solar TPTC with gas-based nanofluid as heat transfer fluid directly absorbing solar energy has been presented and experimentally tested. Particularly, a lab-scale prototype of TPTC, consisting of 4 m^2 parabolic mirror, coaxial quartz receiver tubes with vacuum in the inner space, blower for nanofluid movement, heat exchanger for heat dissipation and pressure regulation system, has been realized. Furthermore, a working fluid, consisting of air-dispersed CuO nanopowders, has been used.

The experimental campaign showed a problem related to the receiver pipe dirtying, which has been investigated in depth: a FTIR analysis demonstrated a strong relationship between dirtying and humidity of the nanofluid.

Finally, the thermal performance of the prototype has been investigated, reaching the maximum temperature of 180°C into the nanofluid circuit and maintaining a temperature higher than 145°C for about 10 hours in a day of measurement, with a mean efficiency of about 65%.

The first results obtained in this work can be assumed as starting point for further studies on TPTC, aimed to minimize the content of humidity within nanofluid, to obtain a better homogenization of nanopowders into the pipe, to reduce the receiver dirtying and to increase its thermal performance.

Acknowledgements

This work was supported by the Project PON02_00323_3588246 INNOVASOL of Italian Ministry of Education, University and Research.

References

[1] Barlev, D., Vidu, R., Stroeve, P. (2011). Innovation in concentrated solar power, Solar Energy Materials & Solar Cells, 95, 2703–2725.

[2] Bakos, G. C., Ioannidis, I., Tsagas, N. F., & Seftelis, I. (2001). Design, optimisation and conversion-effciency determination of a line-focus parabolic-trough solar-collector (PTC). Applied Energy, 68, 43-50.

[3] Kalogirou, S. A. (2004). Solar thermal collectors and applications. Progress in Energy and Combustion Science, 30 (3), 231–295.

[4] Kalogirou, S. A. (2012). A detailed thermal model of a parabolic trough collector receiver. Energy, 48, 298-306.

[5] Vignarooban, K., Xinhai Xu, Arvay, Hsu, A., K., Kannan, A.M., Heat transfer fluids for concentrating solar power systems – A review, Applied Energy, Volume 146, 15 May 2015, Pages 383-396.

[6] Liang, H., You, S., Zhang, H., Comparison of different heat transfer models for parabolic trough solar collectors, Applied Energy, Volume 148, 15 June 2015, Pages 105-114.

[7] Nunes, V.M.B., Queirós, C.S., M.J.V. Lourenço, Santos, F.J.V., Nieto de Castro, C.A, (2016). Molten salts as engineering fluids – A review: Part I. Molten alkali nitrates, Applied Energy, Volume 183, 1 December 2016, Pages 603-611.

[8] Le Brun, N., Hewitt, G.F., Markides C.N., Transient freezing of molten salts in pipe-flow systems: Application to the direct reactor auxiliary cooling system (DRACS), Applied Energy, Volume 186, Part 1, 15 January 2017, Pages 56-67.

[9] Piemonte, V., De Falco, M., Tarquini, P., Giaconia, A. (2011). Life Cycle Assessment of a high temperature molten salt concentrated solar power plant, Solar Energy, 85, 1101–1108

[10] Slocum, A.H., Codd, D.S., Buongiorno, J., Forsberg, C., McKrell, T., Nave, J., Papanicolas, C.N., Ghobeity, A., Noone, C.J., Passerini, S., Rojas, F., Mitsos, A. (2011). Concentrated solar power on demand, Solar Energy, 85, 1519–1529.

[11] de Risi, A., Milanese, M., & Laforgia, D. (2013). Modelling and optimization of transparent parabolic trough collector based on gas-phase nanofluids. Renewable Energy, 58, 134-139.

[12] Xu, G., Chen, W., Deng, S., Zhang, X., & Zhao, S. (2015). Performance Evaluation of a Nanofluid-Based Direct Absorption Solar Collector with Parabolic Trough Concentrator. Nanomaterials, 5(4), 2131–2147.

[13] Gupta, H.K., Agrawal, G.D., Mathur, J., Investigations for effect of Al2O3–H2O nanofluid flow rate on the efficiency of direct absorption solar collector, Case Studies in Thermal Engineering, Volume 5, March 2015, Pages 70-78.

[14] Chen L., Liu, J., Fang, X., Zhang, Z., Reduced graphene oxide dispersed nanofluids with improved photo-thermal conversion performance for direct absorption solar collectors, Solar Energy Materials and Solar Cells, Volume 163, April 2017, Pages 125-133.

[15] Menbari, A., Alemrajabi, A.A., Rezaei, A., Experimental investigation of thermal performance for direct absorption solar parabolic trough collector (DASPTC) based on binary nanofluids, Experimental Thermal and Fluid Science, Volume 80, January 2017, Pages 218-227.

[16] Milanese, M., Colangelo, G., Cretì, A., Lomascolo, M., Iacobazzi, F., & de Risi, A. (2016). Optical absorption measurements of oxide nanoparticlesfor application as nanofluid in direct absorptionsolar power systems–Part I: Water-based nanofluids behavior. Solar Energy Materials & Solar Cells, 147, 315-320.

[17] Lomascolo, M., Colangelo, G., Milanese, M., & de Risi, A. (2015). Review of heat transfer in nanofluids: Conductive, convective and radiative experimental results. Renewable and Sustainable Energy Reviews, 43, 1182-1198.

[18] Wang, X., Xu, X., & Choi, S. (1999). Thermal conductivity of nanoparticle–fluid mixture. Journal of Thermophys Heat Transfer, 13 (4), 474-480.

[19] Lee, S., Choi, U. S., Li, S., & Eastman, E. A. (199). Measuring Thermal Conductivity of Fluids Containing Oxide Nanoparticles. Journal of Heat Transfer, 121 (2), 280-289.

[20] Das, S., Putra, N., Thiesen, P., & Roetzel, W. (2003). Temperature dependence of thermal conductivity enhancement for nanofluids. Journal of Heat Transfer, 125 (4), 567-574.

[21] Khedka, R. S., Sonawane, S. S., & Wasewar, K. L. (2012). Influence of CuO nanoparticles in enhancing the thermal conductivity of water and monoethylene glycol based nanofluids. International Communications in Heat and Mass Transfer, 39 (5), 665–669.

[22] Colangelo, G., Favale, E., de Risi, A., & Laforgia, D. (2012). Results of experimental investigations on the heat conductivity of nanofluids. Applied Energy , 97, 828–833.

[23] Liu, M. S., Lin, M.-C. C., Huang, I. T., & Wang, C. C. (2006). Enhancement of Thermal Conductivity with CuO for Nanofluids. Chemical Engineering and Technology , 29 (1), 72-77.

[24] Alashkar, A., Gadalla, M., Thermo-economic analysis of an integrated solar power generation system using nanofluids, Applied Energy, Volume 191, 1 April 2017, Pages 469-491.

[25] Li, C. H., & Peterson, G. P. (2006). Experimental investigation of temperature and volume fraction variations on the effective thermal conductivity of nanoparticle suspensions (nanofluids). Jornal of Applied Physics, 99 (8), 1-8.

[26] Mintsa, H. A., Roy, G., Nguyen, C. T., & Doucet, D. (2009). New temperature dependent thermal conductivity data for water-based nanofluids. International Journal of Thermal Sciences , 48, 363–371.

[27] Mwesigye, A., Huan, Z., Meyer, J.P., Thermodynamic optimisation of the performance of a parabolic trough receiver using synthetic oil–Al2O3 nanofluid, Applied Energy, Volume 156, 2015, 398-412.

[28] Milanese, M., Colangelo, G., Cretì, A., Lomascolo, M., Iacobazzi, F., & de Risi, A. (2016). Optical absorption measurements of oxide nanoparticles for application as nanofluid in direct absorption solar power systems – Part II: ZnO, CeO2, Fe2O3 nanoparticles behavior. Solar Energy Materials and Solar Cells , 147, 321-326.

[29] Cretì, A., Epifani, M., Taurino, A., Catalano, M., Casino, F., Lomascolo, M., et al. (2013). Optical Absorption Measurements at High Temperature (500 °C) of Oxide Nanoparticles for Application as Gas-Based Nanofluid in Solar Thermal Collector Systems. Advanced Materials Research , 773, 80-86.

[30] Abdelrahman P, Fumeaux P, Suter P. Study of solid-gas suspension used for direct absorption of concentrated solar radiation. Solar Energy 1979; 22:45-8.

[31] Oman J, Novak P. Volumetric absorption in gas-properties of particles and particle-gas suspension. Solar Energy, 1996; 56(6):597-606.

[32] Zhang, H., Benoit, H., Gauthier, D., Degrève, J., Baeyens, J., López, I.p., Hemati, M., Flamant, G., Particle circulation loops in solar energy capture and storage: Gas–solid flow and heat transfer considerations, Applied Energy, Volume 161, 1 January 2016, Pages 206-224.

[33] Miller FJ, Koenigsdorff RW. Thermal modeling of a small-particle solar central receiver. Journal of Solar Energy Engineering 2000;122:23-9.

[34] Bertocchi R, Karni J, Kribus A. Experimental evaluation of a non-isothermal high temperature solar particle receiver. Energy 2004;29:687-700.

[35] J.A. Duffie, W.A. Beckman, Solar Engineering of Thermal Processes, second ed., Wiley Interscience, New York, 1991. pp. 358–361.

[36] F. Incropera, D.P. De Witt, Fundamentals of Heat and Mass Transfer. s.l. : Wiley & Sons Ltd., 2006.

[37] Warren, S., Flavell, F. W., Thomas, A. G., Hollingworth, J., Dunwoody, P. M., Downes, S., et al. (1999). Adsorption of H2O on single crystal CuO. Surface Science , 436, 1-8.

[38] Henrich, V. E., & Cox, P. A. (1996). The Surface Science of Metal Oxides. Cambridge: Cambridge University Press.

[39] Raghavachari, K., Chabal, Y. J., & Struck, L. M. (1996). Vibrational interactions at surfaces: H2O on S i(100). Chemical Physics Letters , 252, 230-235.

[40] Salman, S. A., & Katırcıoglu, S. (1998). Adsorption of water on stepped Si(100) surface. Surface Science , 416, 9–16.

[41] Maréchal, Y. (2011). The molecular structure of liquid water delivered by absorption spectroscopy in the whole IR region completed with thermodynamics data. Journal of Molecular Structure , 1004 (1-3), 146–155.

[42] Bergonzi, I., Mercury, L., Brubach, J.-B., & Roy, P. (2014). Gibbs free energy of liquid water derived fromi nfrared measurements. Physical Chemistry Chemical Physics , 16, 24830-24840.

[43] Naccarato, F., Potenza, M., de Risi, A., Stigliano, G., Numerical Optimization of an Organic Rankine Cycle Scheme for Co-generation, International Journal of Renewable Energy Research, vol. 4, n. 2, 2014.

[44] Jiang, L., Lu, H.T., Wang, L.W., Gao, P., Zhu, F.Q., Wang, R.Z., Roskilly, A.P., Investigation on a small-scale pumpless Organic Rankine Cycle (ORC) system driven by the low temperature heat source, Applied Energy, Volume 195, 1 June 2017, Pages 478-486.

[45] Ziviani, D., Gusev, S., Lecompte, S., Groll, E.A., Braun, J.E., Horton, W.T., van den Broek, M., De Paepe, M., Optimizing the performance of small-scale organic Rankine cycle that utilizes a single-screw expander, Applied Energy, Volume 189, 1 March 2017, Pages 416-432.

[46] Ji D.K., Lee, S., Kim, J., Kim, M.S., Kim, M.S.,Parametric study and performance evaluation of an organic Rankine cycle (ORC) system using low-grade heat at temperatures below 80 °C, Applied Energy, Volume 189, 1 March 2017, Pages 55-65.

[47] Zhang, Q., Li, X., Chang, C., Wang, Z., & Liu, H. (2013). An experimental study: Thermal performance of molten salt cavity. Applied Thermal Engineering , 50, 334-341.

[48] Barcia, L. A., Menéndez, R. P., Esteban, J. M., Prieto, M. J., Ramos, J. M., de Cos Juez, F. J., et al. (2015). Dynamic Modeling of the Solar Field in Parabolic. Energies , 8, 13361–13377.

Figures

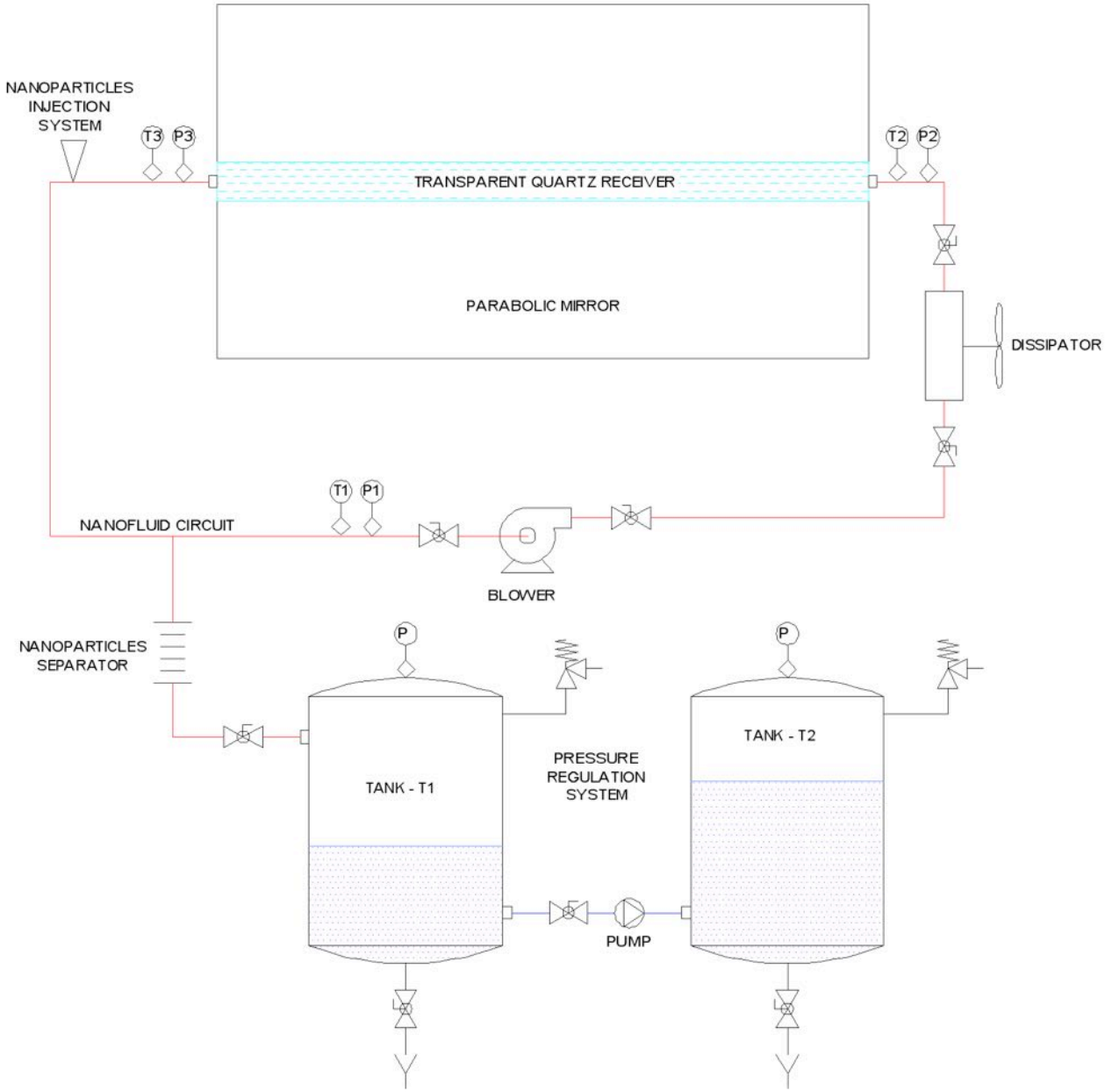

Figure 1. Layout of the prototype of TPTC.

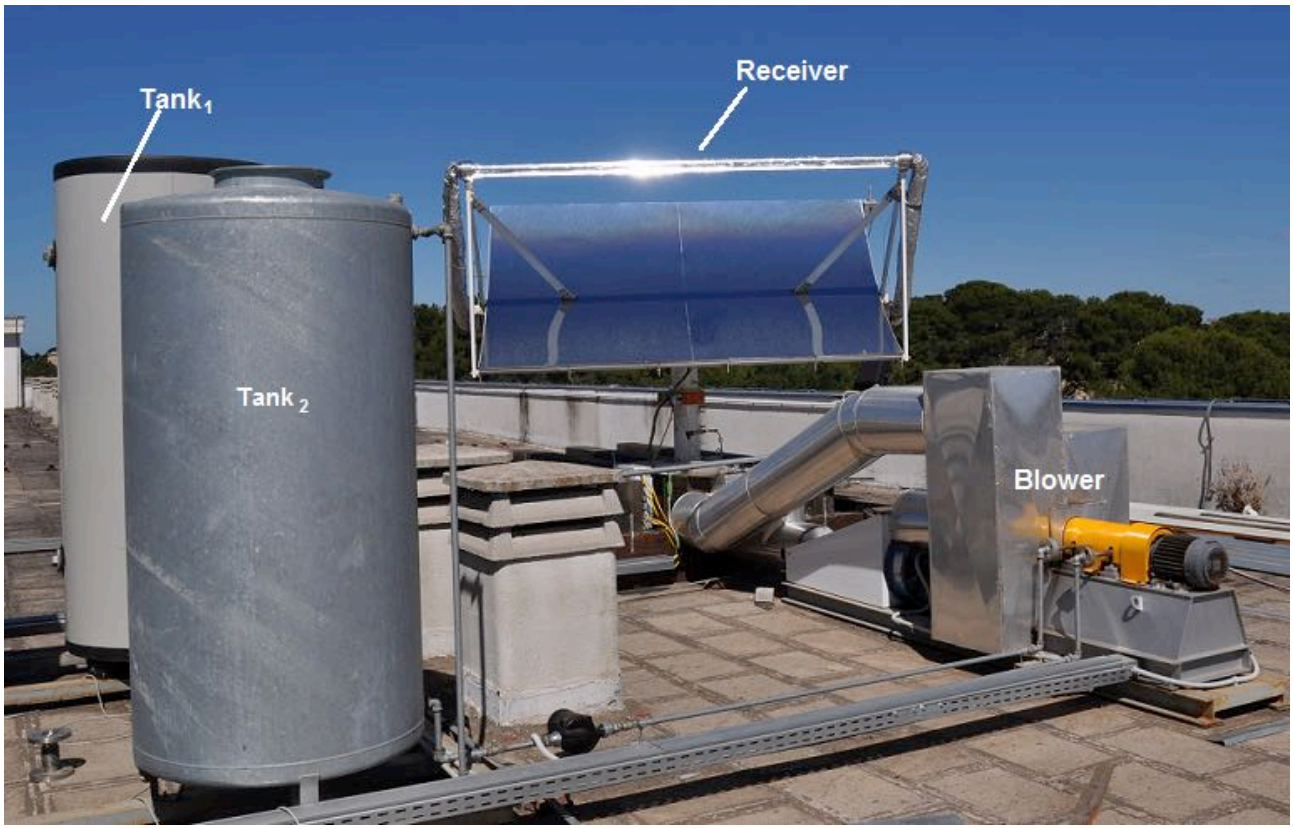

Figure 2. Image of the prototype of TPTC.

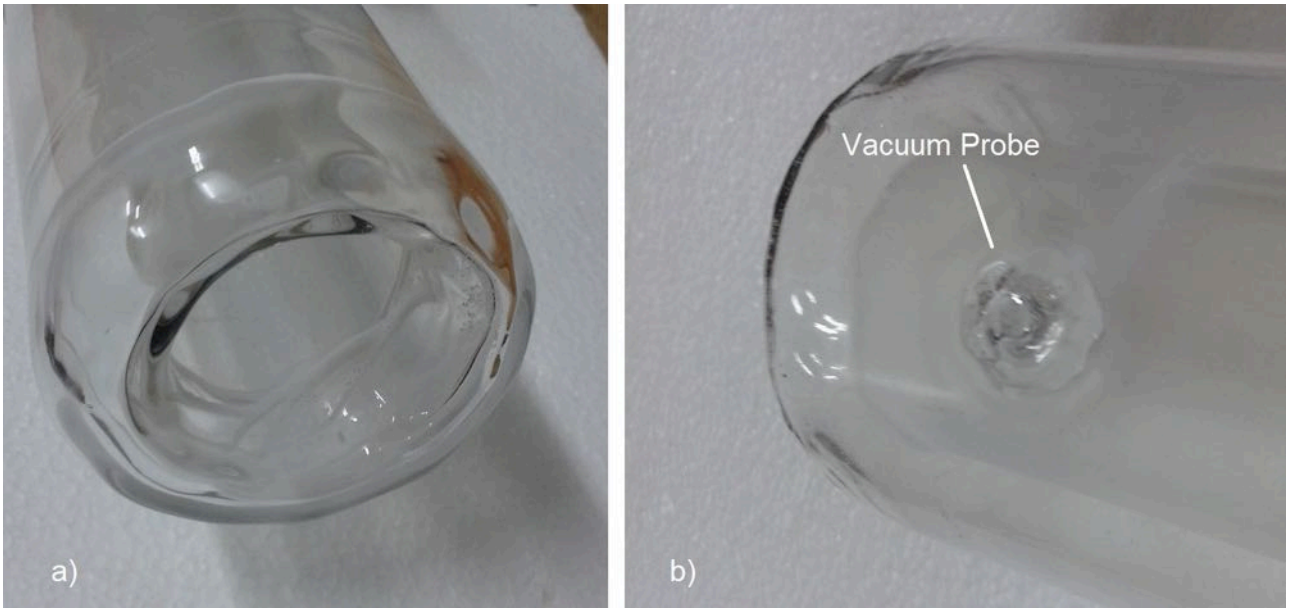

Figure 3. Transparent coaxial quart pipes

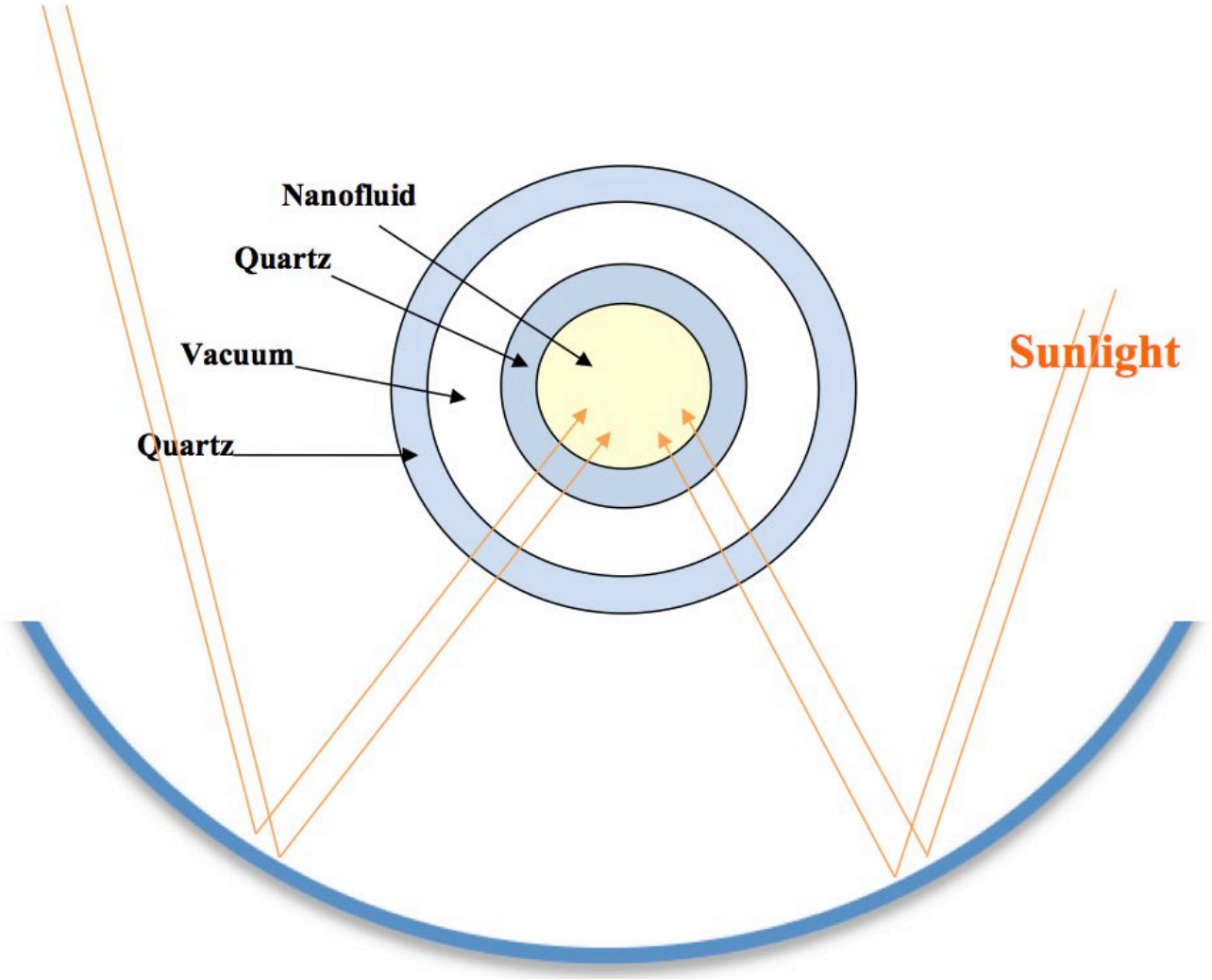

Figure 4. Optical scheme of the transparent receiver

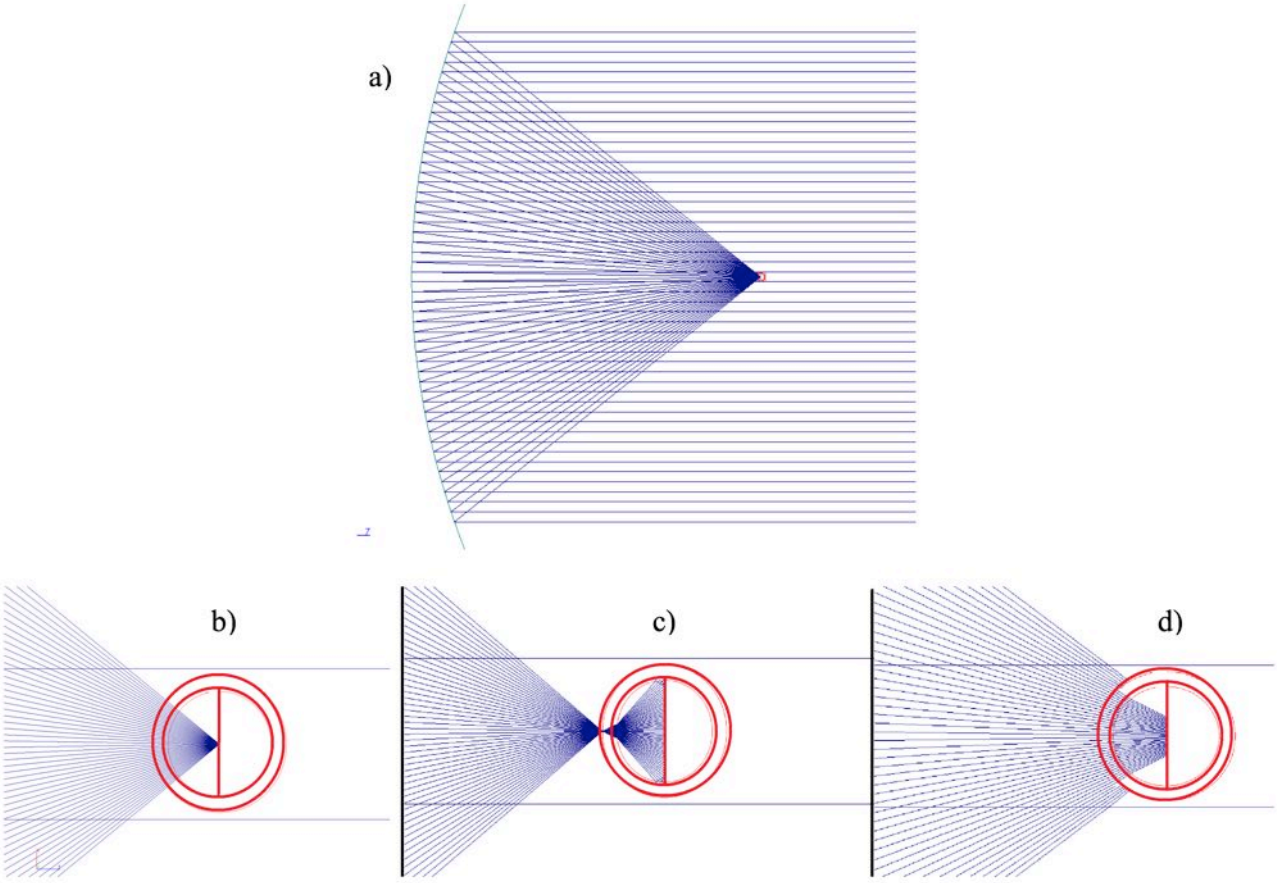

Figure 5. Raytracing analysis: a), b) the focus is placed at a distance of 1000 mm from the base of the mirror; c) focus at 1010 mm from the base of the mirror; d) focus at 990 mm from the base of the mirror.

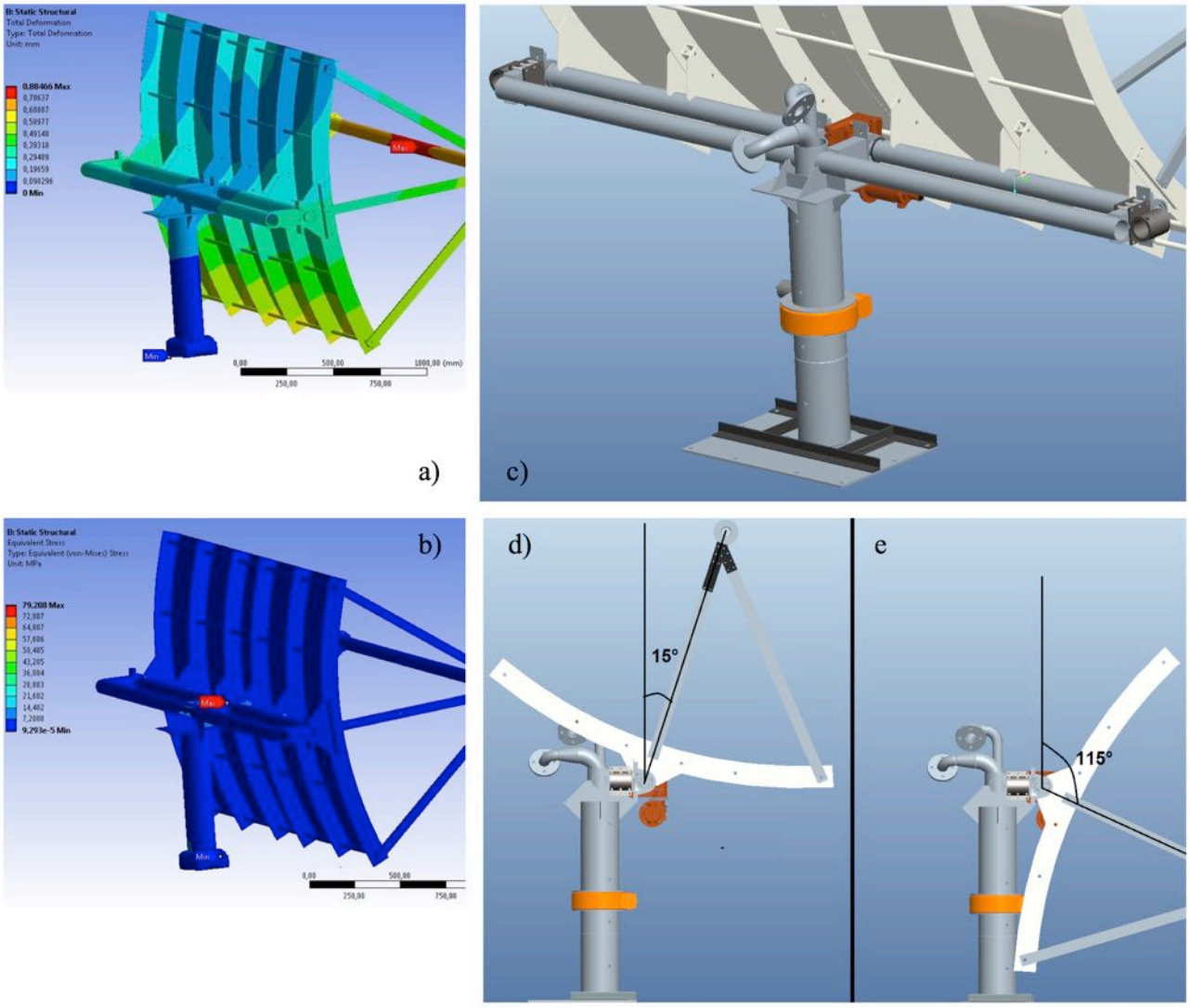

Figure 6. Design of the prototype: a) and b) maximum deformation and Von Mises stress under the effects of high speed wind conditions (140 km/h); c) isometric view of solar tracker; d) maximum elevation solar tracker; e) minimum elevation solar tracker.

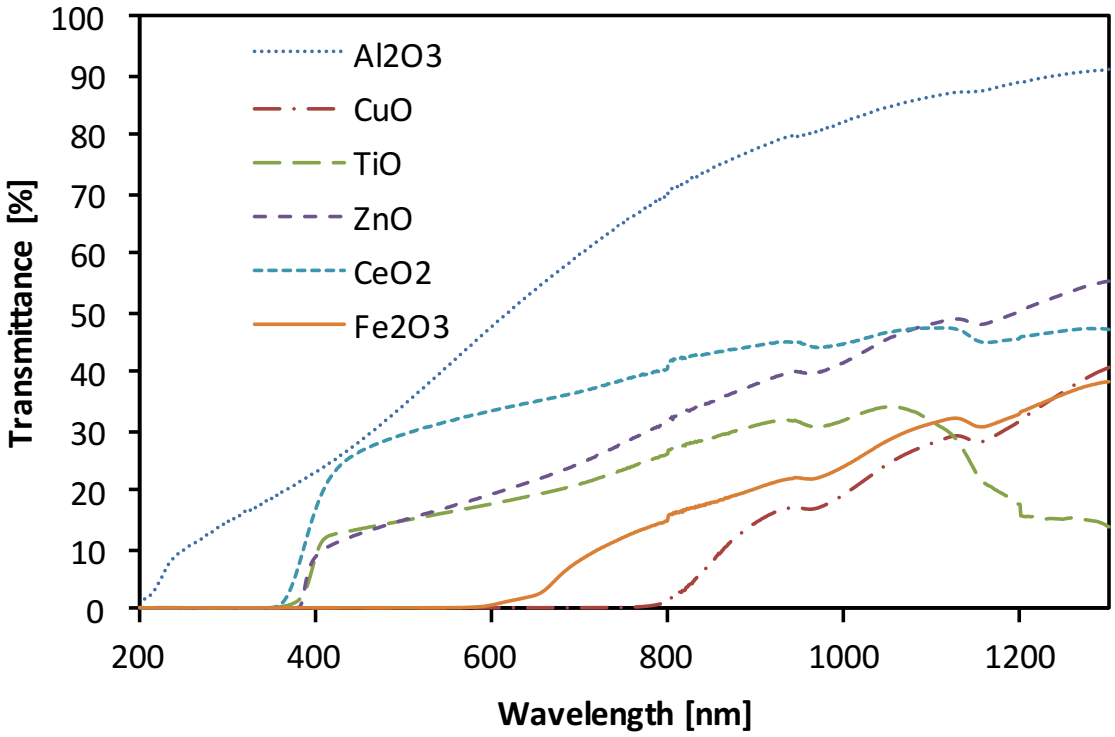

Figure 7. Transmittance behavior as function of wavelength for several nanofluids (*NPs* concentration 0.05%vol) [16].

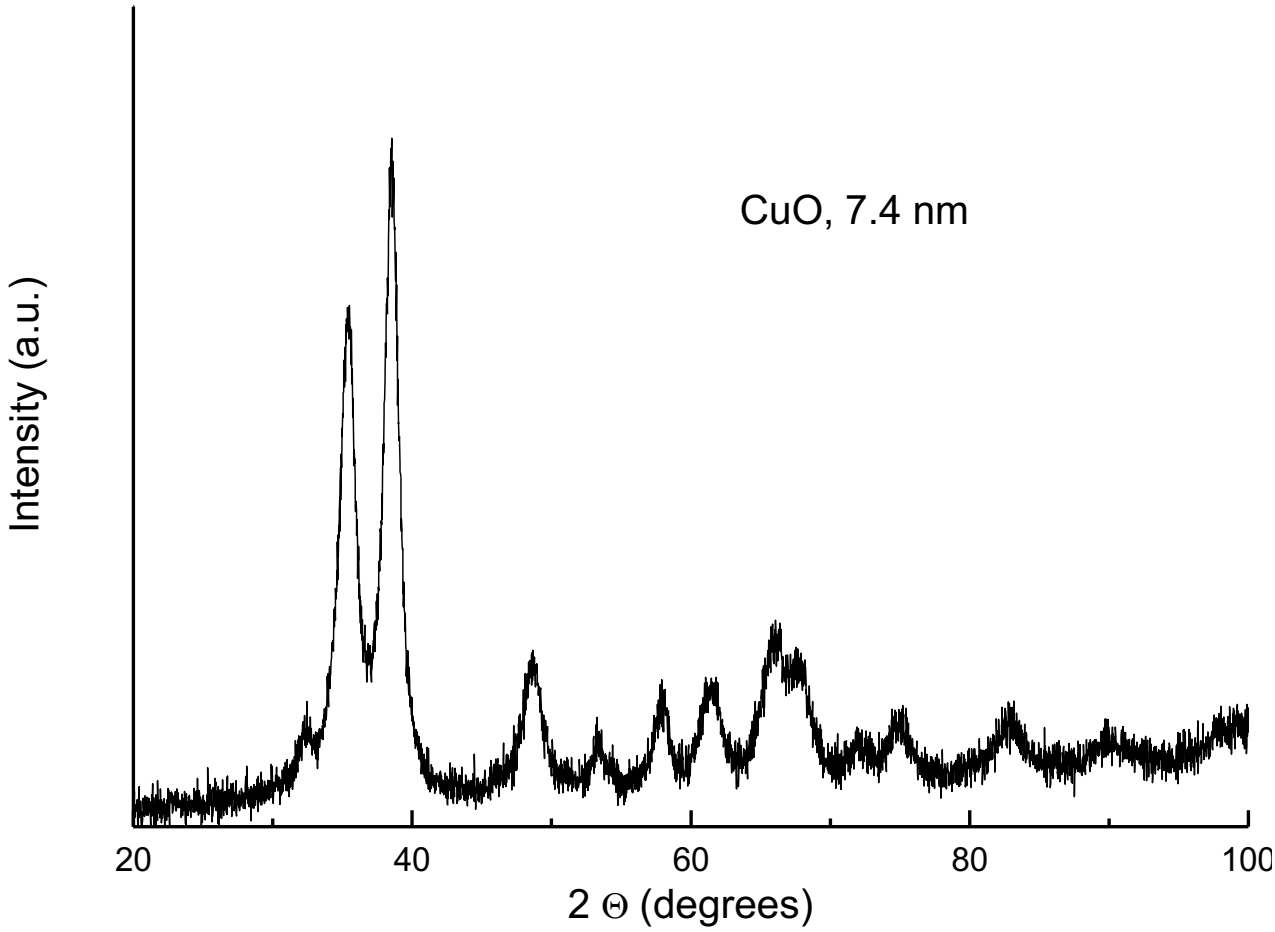

Figure 8: XRD spectrum of CuO *NPs.*

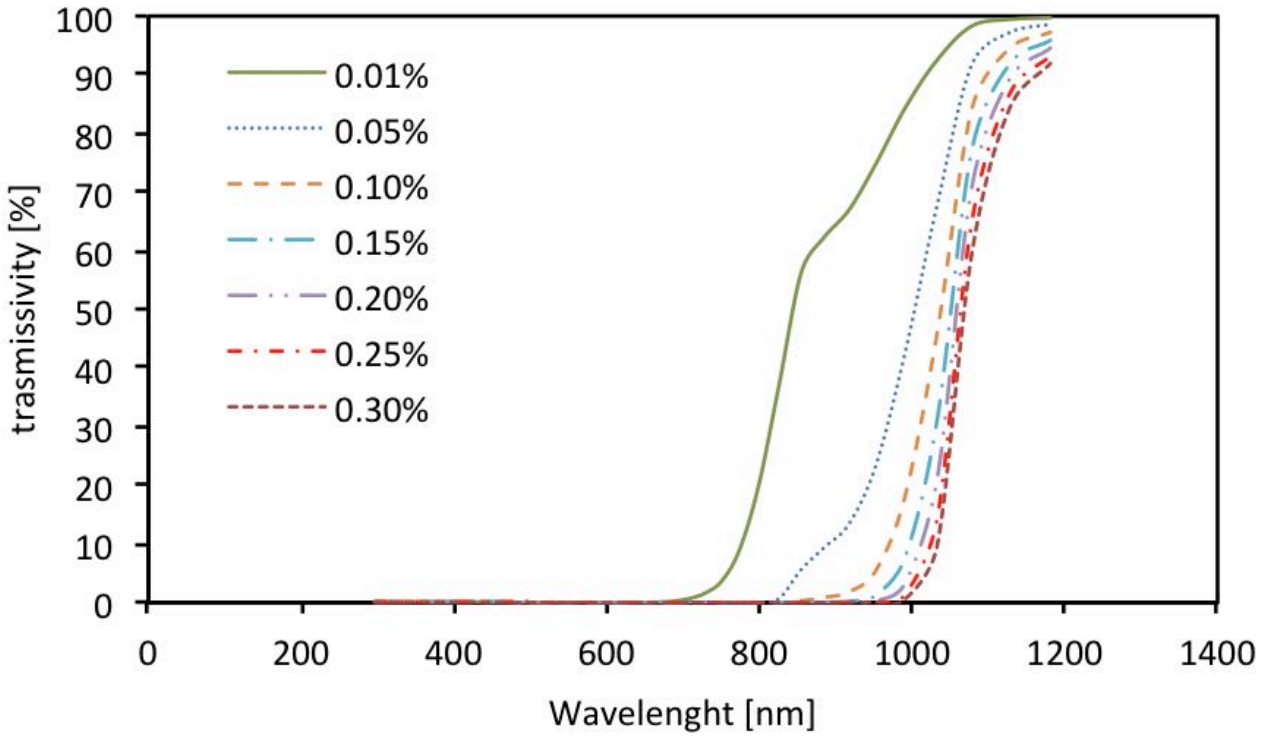

Figure 9. NF trasmissivity as a function of wavelength for several *NPs* concentration (%vol) within *NF*.

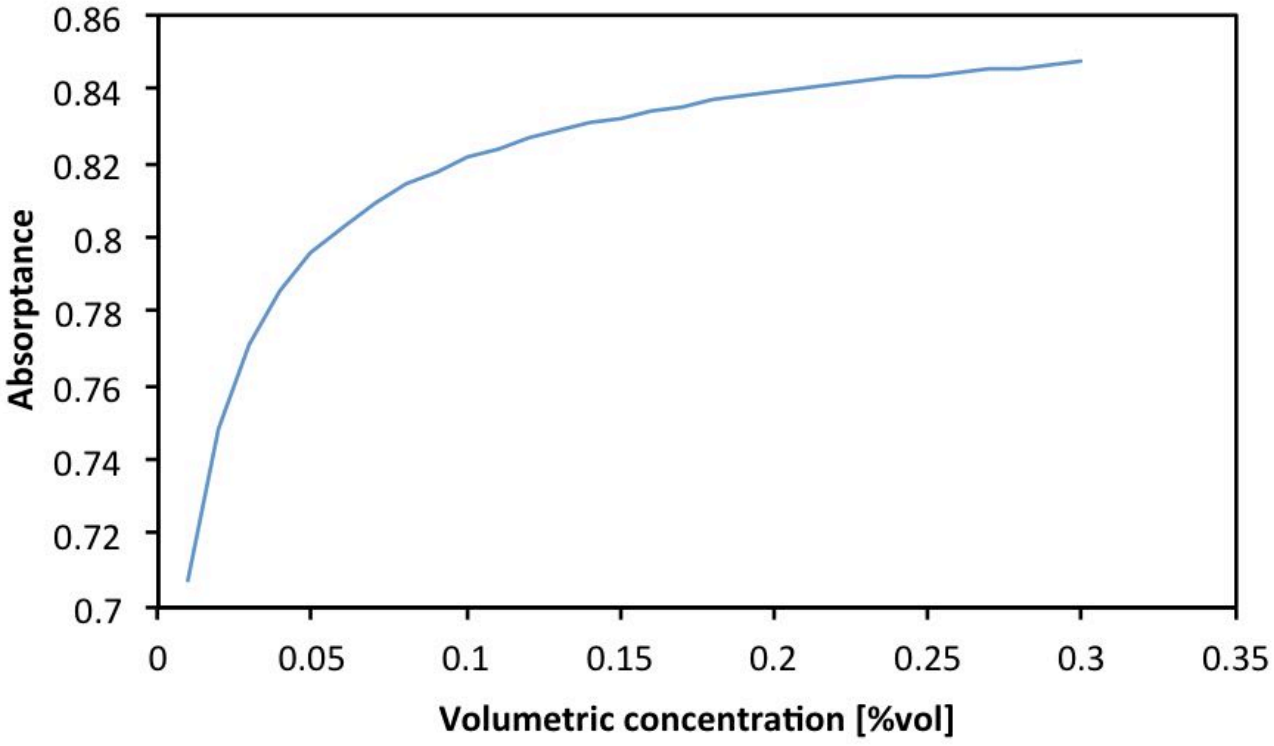

Figure 10. Mean receiver quartz tube absorptance as a function of the volumetric concentration of *NPs* within *NF*.

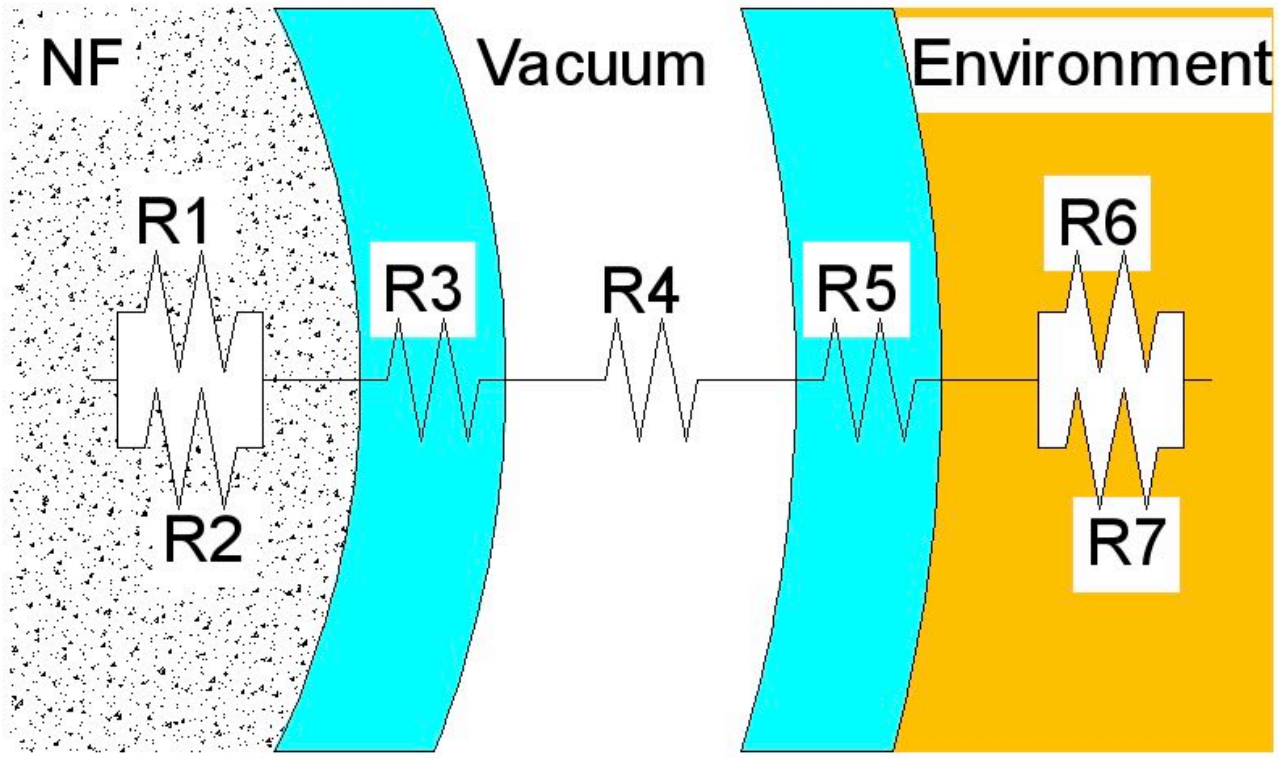

Figure 11. Scheme for total resistance to heat transfer.

Figure 12. Nanopowder deposition within the metallic pipe

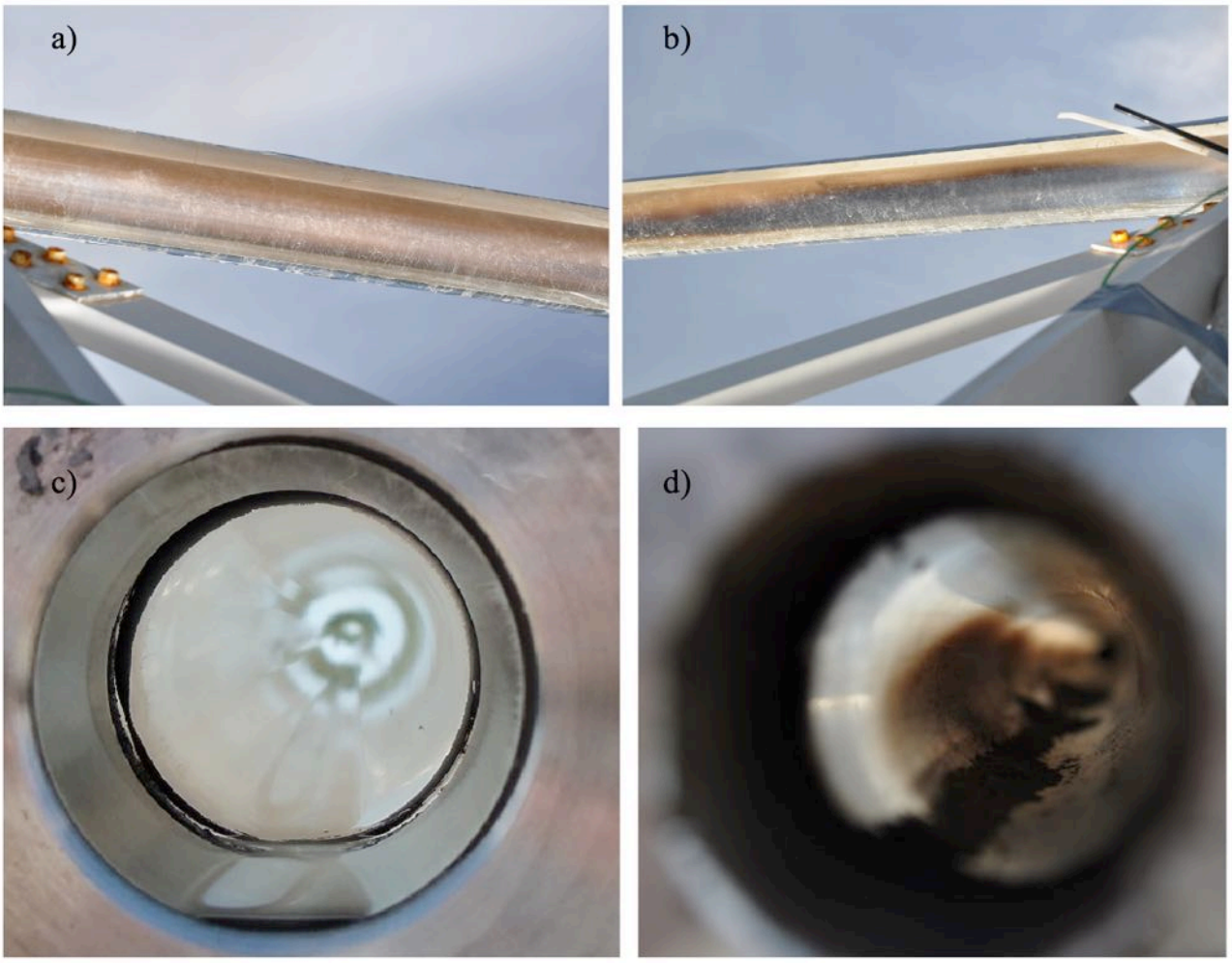

Figure 13. Nanopowder deposition in the receiver: a) outlet; b) inlet; c) close to the inlet section, before the first run; d) close to the inlet section, after 900 hours of operation.

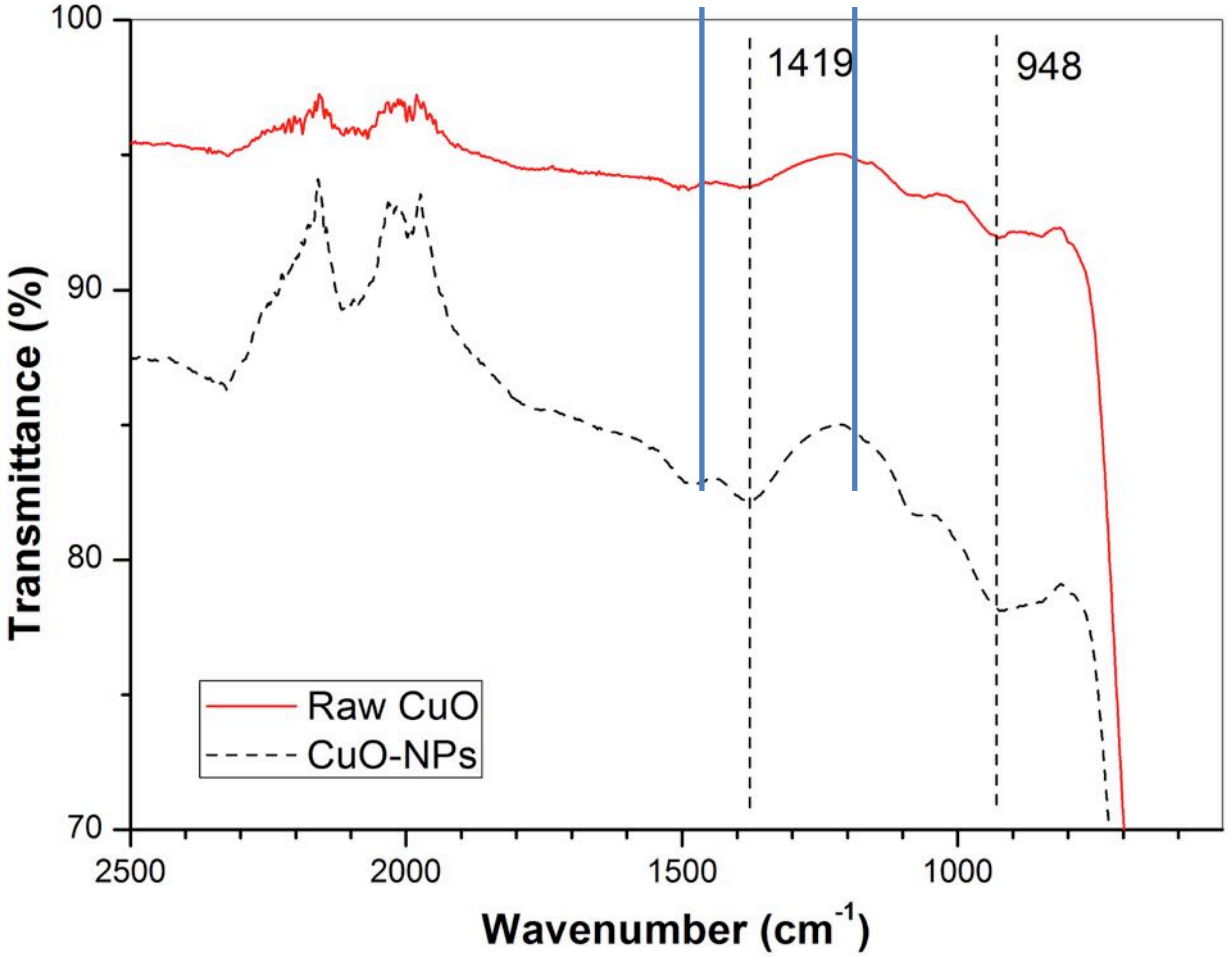

Figure 14. FTIR spectrum of raw CuO (solid curve) and CuO powder from the receiver (dashed curve) after 300 hours of operation.

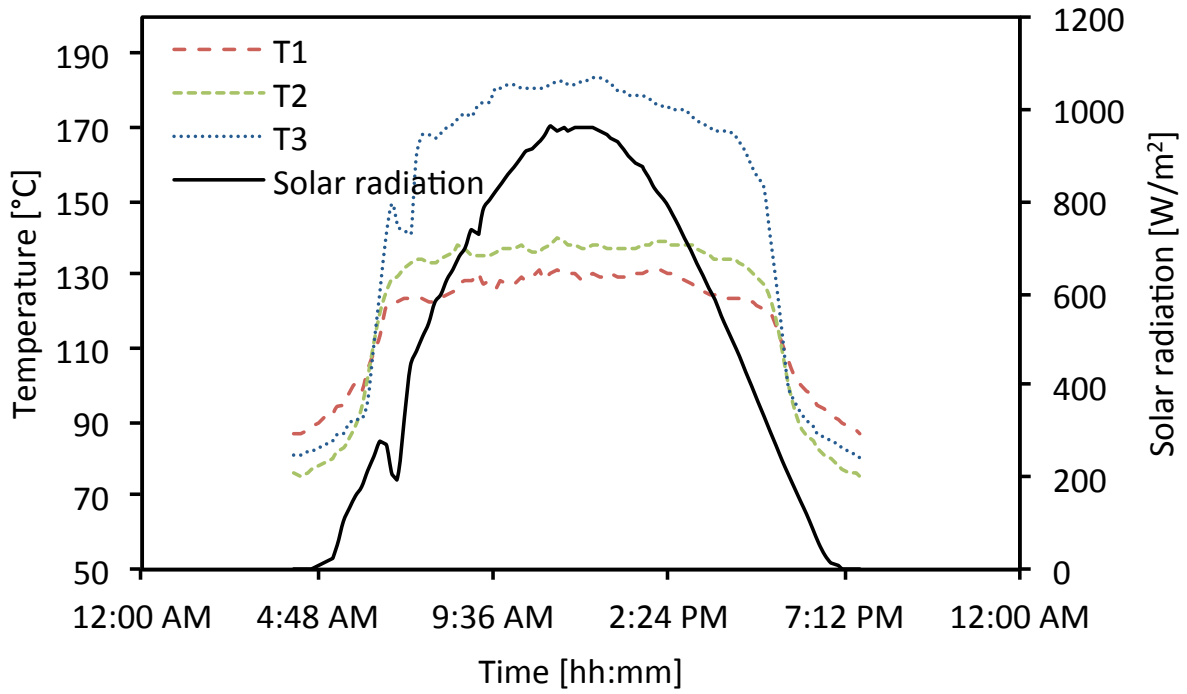

Figure 15. Measured *NF* temperatures and solar radiation

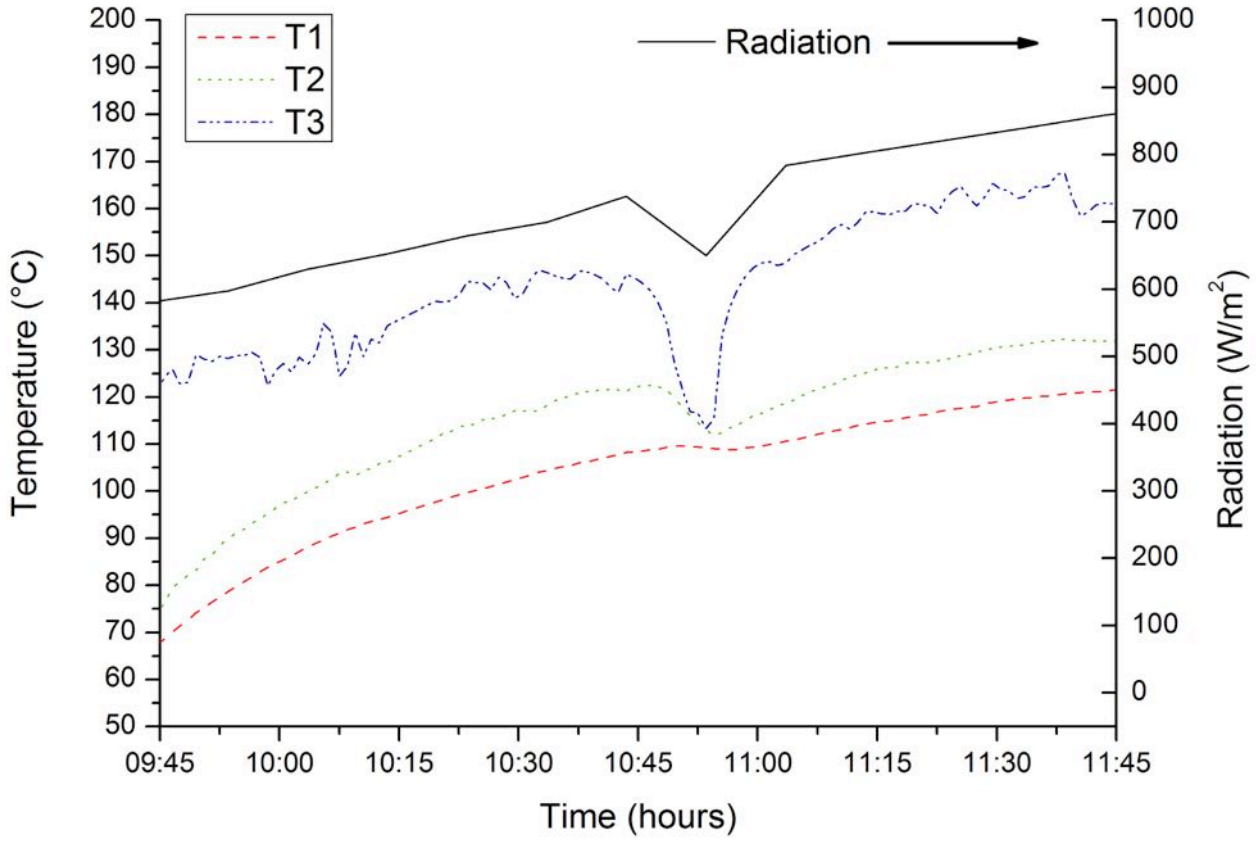

Figure 16. Weather conditions influence on *NF* temperature

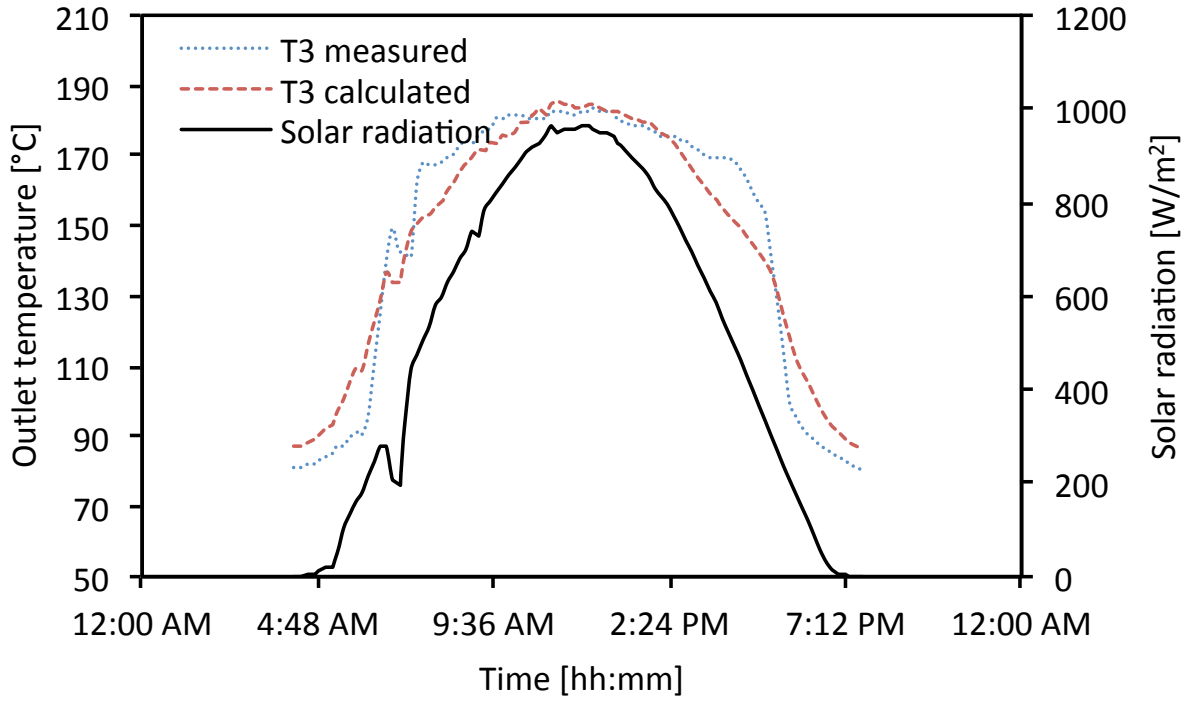

Figure 17. Comparison between experimental and calculated outlet temperature T3 in the prototype

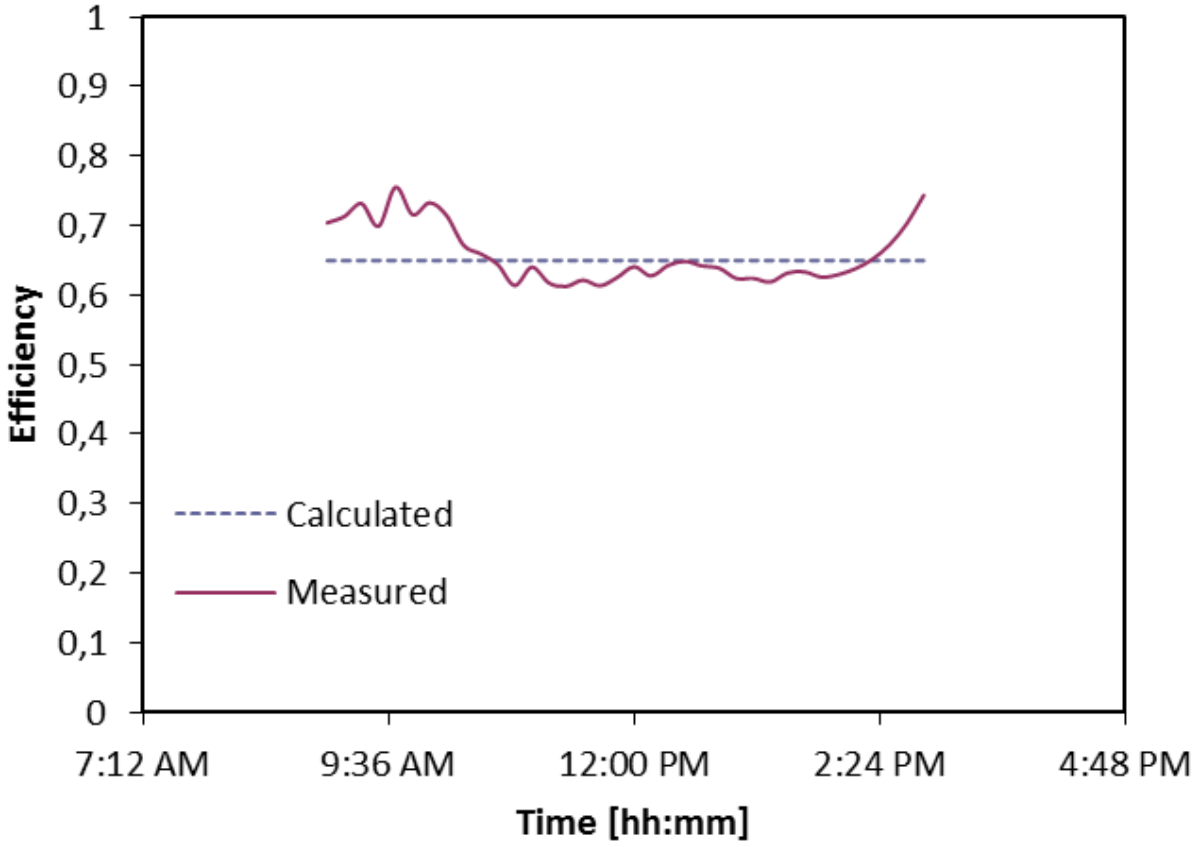

Figure 18. Comparison between experimental and calculated efficiency of the prototype

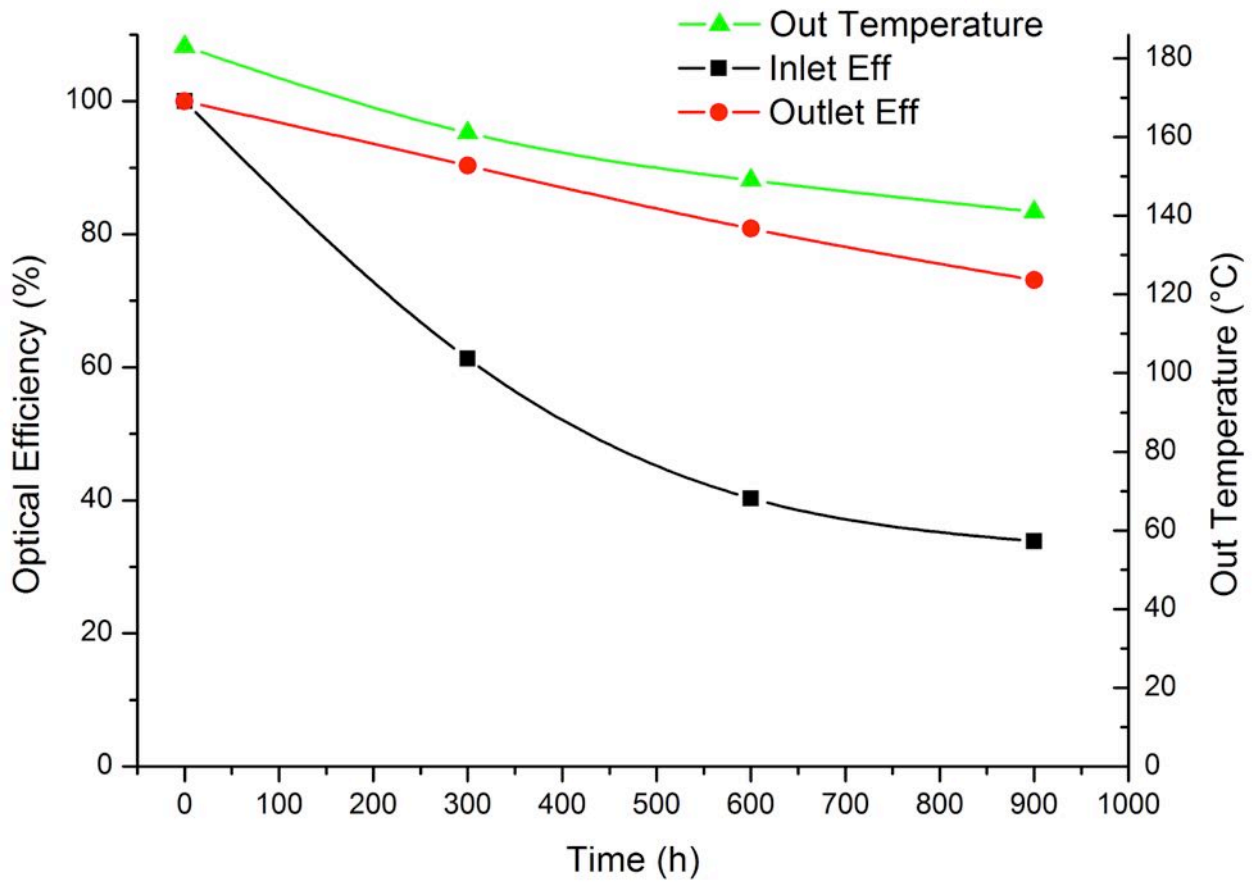

Figure 19. Optical efficiency of the receiver pipe (inlet and outlet) and temperature (only outlet) as a function of time of operation

Tables

Table 1. Main characteristics of the transparent receiver

Description	Value
Inner diameter of the internal tube	0.040 m
Inner diameter of the external tube	0.076 m
Internal and external tube thickness	0.003 m
Vacuum thickness	0.015 m
Internal and external tube thermal conductivity	2 W/m K
Quartz emissivity	0.8

Table 2. Parameters of numerical analysis. (*) Measured values.

Description	Value
NF velocity (*)	11.5 m/s
NF mass flow rate (*)	0.068 kg/s
NPs volume concentration (*)	0.06 %vol
Incidence angle of solar radiation, θ	0 rad
Outside air temperature	298.2 K
Wind velocity	4 m/s